

Conditional Activation of Fibroblast Growth Factor Receptor (FGFR) 1, but not FGFR2, in Prostate Cancer Cells Leads to Increased Osteopontin Induction, Extracellular Signal-regulated Kinase Activation, and *in Vivo* Proliferation¹

Kevin W. Freeman, Rama D. Gangula, Bryan E. Welm,² Mustafa Ozen, Barbara A. Foster, Jeffrey M. Rosen, Michael Ittmann, Norman M. Greenberg, and David M. Spencer³

Departments of Immunology [K. W. F., R. D. G., D. M. S.], Cell and Molecular Biology [B. E. W., B. A. F., J. M. R., N. M. G.], and Pathology [M. O., M. I.], Baylor College of Medicine, Houston, Texas 77030

ABSTRACT

Changes in the fibroblast growth factor receptor (FGFR) axis are often associated with prostate cancer (CaP) progression. We have used chemically induced dimerization (CID) to elucidate the individual contributions of FGFR1 and FGFR2 to tumor etiology. Novel CaP cell lines stably expressing CID/AP20187-inducible FGFR1 (iFGFR1) and iFGFR2 were made using the tumorigenic transgenic adenocarcinoma of the murine prostate (TRAMP)-derived clone, TRAMP-C2N (C2N), to generate C2N.iFGFR1 or C2N.iFGFR2 cells. To test the effects of iFGFR activation on tumor growth, mice bearing s.c. C2N.iFGFR1- or C2N.iFGFR2-derived tumors were treated biweekly with CID. Activation of iFGFR1 led to rapid tumor growth as a result of increased proliferation. In contrast, expression of iFGFR2 inhibited tumor growth. Furthermore, we have ascertained that FGFR1 activation appears to be most important during the early stages of tumor development, but once established, tumors become rapidly CID independent. In these C2N-based lines, quantitative signaling differences were seen between the two receptors, with iFGFR1 leading to more robust extracellular signal-regulated kinase activation. Additionally, activation of iFGFR1, but not iFGFR2, led to strong up-regulation of osteopontin, a secreted glycoprotein involved in integrin activation and associated with CaP progression and metastasis. These studies support the hypothesis that observed changes in the FGFR axis in mammals during CaP progression are causally important.

INTRODUCTION

Despite causing approximately 30,000 deaths a year in the United States (1), there is still a paucity of information concerning the signaling pathways that influence CaP⁴ progression and metastasis. FGF signaling, mediated by up to four distinct FGFRs, can lead to multiple outcomes, including proliferation, differentiation, survival, and migration in various tissues (2) and has been implicated in CaP progression. A model of FGF signaling in normal prostate tissue proposes that androgen-induced stromal-derived FGF7 activates epithelial-restricted FGFR2IIIb to maintain survival, growth, and differentiation of the prostate epithelium (3). As observed in both rodent models for CaP and humans, FGFRs undergo reproducible changes during the progression toward metastatic disease characterized by an isoform change or complete loss of FGFR2 (4), concomitant with ectopic expression of FGFR1 (5–9). Independence from stroma-derived FGFs occurs when up-regulated epithelium-derived FGFs

cause autocrine signaling through FGFR1 (3). Moreover, introduction of a dominant negative FGFR1 leads to cell death in PC-3, LNCaP, and DU145 CaP cell lines, supporting a causal role for aberrant FGFR1 expression in transformation (10). Furthermore, the cytoplasmic signaling domain of FGFR1 promotes the growth of s.c. Dunning rat CaP cell line-derived tumors, whereas that of homologous FGFR2 promotes differentiation (5, 6). However, these studies could not differentiate between a transient effect and a continuous role for FGFR1 signaling in supporting tumor growth.

To resolve the role of FGFR1 and FGFR2 in CaP tumor growth and progression, we have used CID to temporally control FGFR signaling in transplant tumors. In CID, a lipid-permeable, synthetic dimerizing drug, such as AP20187, is used to noncovalently bind and oligomerize modified CID-binding domains, such as FK506 binding protein 12 KD (FKBP12), that are genetically fused to the target protein domains. In turn, CID removal terminates signaling. Hence, CID allows the conditional and reversible activation of target proteins when target proteins are naturally activated via oligomerization (11–14). Using CID, we could directly determine the quantitative or qualitative signaling differences between FGFR1 and FGFR2 in CaP-derived cells.

Here we describe the application of iFGFRs to temporal studies of the role of the FGFR axis in tumor progression using prostate tumor cell (15) lines derived from the TRAMP model (16–18). We demonstrate that iFGFR1 affects tumor “establishment” and early growth of transplanted prostate tumors in syngeneic hosts by promoting proliferation. However, at later stages of tumor development, iFGFR1 no longer promotes tumor growth. In contrast, iFGFR2 appears to interfere with tumor establishment and growth. Additionally, FGFR1 activation leads to higher Erk phosphorylation than FGFR2 and up-regulation of the metastasis-associated protein OPN, which may be responsible for some of the selective tumor-promoting effects of iFGFR1.

MATERIALS AND METHODS

Plasmid Constructs. The vector pSH1/M-FGFR1-F_vF_{vis}-E was created as described previously and vector pSH1/M-FGFR2-F_vF_{vis}-E was created using the same strategy as described previously using forward primer 5'-AATTA-CTCGAGGACTTCAGCAGCCAGCCAGCT-3' and reverse primer 5'-AGTTCAGTCGACTGTTTAACACTGCCGTTTATGTGTG-3' (19). Briefly, the cytoplasmic signaling domains of FGFR1 and FGFR2 were PCR amplified with *Xho*I and *Sal*I flanking sites and cloned into parent expression vector pSH1/M-F_vF_{vis}-E (20).

Cell Lines. TRAMP-C2N and TRAMP-C1A are subclones of TRAMP-C2 and TRAMP-C1, respectively (15), derived from a primary tumor of the TRAMP model (17, 21). To establish C2N and C1A subclones expressing iFGFRs, cells were transfected with linearized pSH1/M-FGFR1-F_vF_{vis}-E, pSH1/M-FGFR2-F_vF_{vis}-E, or pSH1/MF_vF_{vis}-E plus vector pBJ5-Neo at a 10:1 ratio using FuGENE-6 (Roche Applied Sciences, Indianapolis, IN) following the manufacturer's instructions. All TRAMP-derived cell lines were cultured as described previously (15). Clonal iFGFR cell lines were derived by limiting dilution. For all *in vitro* experiments, cells were grown to confluence in

Received 11/6/02; revised 6/23/03; accepted 7/22/03.

The costs of publication of this article were defrayed in part by the payment of page charges. This article must therefore be hereby marked *advertisement* in accordance with 18 U.S.C. Section 1734 solely to indicate this fact.

¹ Supported by NIH Grants R01 CA87569 and U01 CA84296 and NIH Training Grant T32-AI07495 (to K. W. F.).

² Present address: Department of Anatomy, University of California San Francisco, San Francisco, CA 94143.

³ To whom requests for reprints should be addressed, at Baylor College of Medicine, One Baylor Plaza/M929, Houston, TX 77030. E-mail: dspencer@bcm.tmc.edu.

⁴ The abbreviations used are: CaP, prostate cancer; CID, chemically induced dimerization; TRAMP, transgenic adenocarcinoma of the murine prostate; FGF, fibroblast growth factor; FGFR, fibroblast growth factor receptor; iFGFR, inducible fibroblast growth factor receptor; OPN, osteopontin; VEGF, vascular endothelial growth factor; Erk, extracellular signal-regulated kinase; HRP, horseradish peroxidase; HA, hemagglutinin.

100-mm tissue culture plates, washed twice with DMEM, and serum starved for 48 h in DMEM unless otherwise stated.

Western Blot Analysis and Immunoprecipitation. After starving cells, a time course was done with addition of AP20187 (100 nM) or serum (10%-containing media). Immunoblotting was carried out as described previously (14). Membranes were incubated with primary antibodies against phospho-Erk, total Erk (Cell Signaling Technology, Beverly, MA), or α -tubulin (Santa Cruz Biotechnology, Santa Cruz, CA) or anti-OPN (Santa Cruz Biotechnology) diluted 1:500 in blocking buffer overnight or anti-HA (HA.11; Covance, Richmond, CA) at 1:1500 for 1 h, followed by a secondary antibody of either HRP-linked polyclonal goat antimouse antibody (1:2000; Santa Cruz Biotechnology) or HRP-linked polyclonal goat antirabbit antibody (1:1000; Santa Cruz Biotechnology) for 30 min. Immunoprecipitation was carried out using the IMMUNOCatcher kit (Cytosignal Research Products, Irvine, CA) following the manufacturer's protocol using 2 μ g anti-phosphotyrosine antibody 4G10 (Upstate Biotechnology, Lake Placid, NY) for immunoprecipitation and HA.11 immunoblotting as described above. Phosphatase inhibitors I and II (Sigma, St. Louis, MO) were added to lysate.

RNAse Protection Assay. RNAse protection assays were performed following the manufacturer's instruction for the RNAse Protection Kit (Roche Applied Sciences). Briefly, murine OPN cDNA was *PfuI* amplified using forward primer 5'-ACAGATTGGCAGTGATTTGCTTTTGCC-3' and reverse primer 5'-ACAGCTTGTCTTGTGGCTGTGAAAC-3' and cloned into pCR-Blunt (Invitrogen, Carlsbad, CA) to make pCR-oste. *PvuII*-linearized pCR-oste and *MunI*-linearized plasmid pA544 containing β -actin (Roche Applied Sciences) were used to synthesize [³²P]CTP-labeled antisense RNA probes of 150 and 255 bp in size, respectively, using the SP6/T7 Transcription Kit (Roche Applied Sciences). Template DNA was digested with RNase-free DNase I, and probes were gel purified before hybridization with 1 μ g of total RNA. Total RNA was isolated using Trizol reagent (Life Technologies, Inc., Gaithersburg, MD) from cells after starvation and incubation with 100 nM AP20187 for various times. Hybridization was carried out for 4 h at 45°C. "Nonprotected" RNA molecules and excess probe were digested with RNase A and T1. "Protected" RNA molecules were purified and resolved on a denaturing polyacrylamide gel, dried, and imaged by X-ray film.

Apoptosis Assay and Proliferation Assays. Cells were grown to confluence in 12-well plates, washed twice with DMEM, and plated in either 10% serum media or with DMEM in triplicate wells \pm 100 nM AP20187. After 22 h of culture, media were removed, and cells received 3 J of UVC using a UV Stratalinker 1800 (Stratagene, La Jolla, CA). Media were replaced, and cells were harvested with a cell scraper 2 h later. Cells were centrifuged and resuspended in 50 μ l of DMEM. An equal volume of cells was mixed with 0.2% trypan blue for live/dead counting. To measure effects on proliferation, 5000 cells were plated in DMEM with log dilutions of AP20187 in duplicate in 96-well plates. After 24 h, a CyQUANT Cell Proliferation Kit (Molecular Probes, Eugene, OR) was used following the manufacturer's protocol. A Titertek Fluoreskan II (ICN Pharmaceuticals, Costa Mesa, CA) was used to measure CyQUANT fluorescence. Probabilities were determined by *t* test.

Immunohistochemistry. Immunohistochemistry was carried out as described previously (18). Slides were incubated with anti-Ki-67 antibody (Novacastra, Newcastle upon Tyne, United Kingdom) at 1:1000 in Power Block for 1 h, followed by incubation with biotin-conjugated goat antirabbit antibody at 1:2000 (Vector Laboratories, Burlingame, CA) for 1 h. Probability was determined by *t* test.

RESULTS

Creation and Testing of iFGFRs. To create chimeric iFGFRs for *in vivo* studies, the intracellular signaling domains of FGFR1 and FGFR2 were subcloned onto the NH₂-terminal side of tandem high-specificity dimerizer drug (*i.e.*, AP20187)-binding proteins, FKBP12_{v36} (F_v) as described previously (19, 22). Membrane localization was achieved using a v-*Src* myristoylation targeting sequence. The chimeric receptors were HA epitope-tagged at the COOH terminus for immunoprecipitation and immunoblotting (Fig. 1A).

Determining Signaling Differences between iFGFR1 and iFGFR2. As a model system to assess the consequences of CID-mediated activation, we stably expressed iFGFR1 and iFGFR2 (and

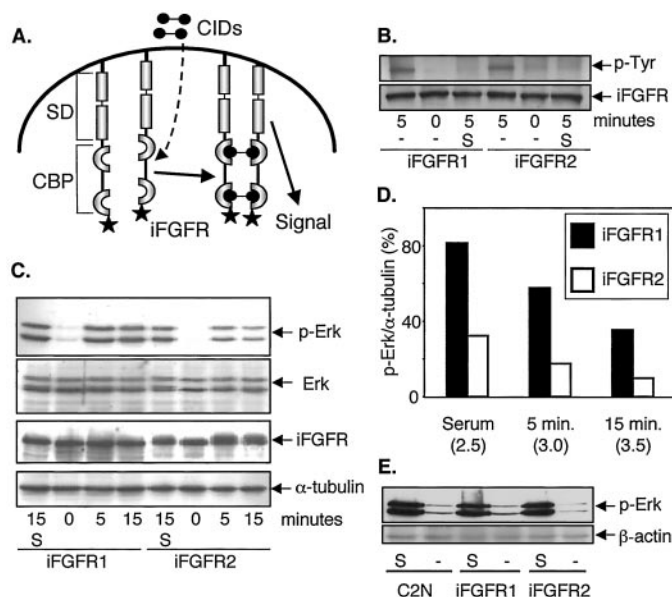


Fig. 1. Equivalent activation of iFGFR1 and iFGFR2 leads to quantitative differences in activation of downstream targets. *A*, diagram of CID-iFGFR proteins, in which lipid-permeable AP20187 passes through the plasma membrane, leading to targeted oligomerization and activation of myristoylated FGFR cytoplasmic signaling domains (SD) fused to tandem CID-binding proteins (CBP). C2N.iFGFR1 and C2N.iFGFR2 cells were treated at various times with 100 nM AP20187 (*B* and *C*) or 10% serum [S (*B*, *C*, and *E*)]. *B*, cells were lysed with strong detergent, and 5% of supernatant was used as input control by immunoblotting with anti-HA antibodies (*bottom panel*). Remaining supernatant was used for immunoprecipitation with anti-phosphotyrosine antibody, 4G10, followed by immunoblotting with anti-HA antibodies (*top panel*). *C*, C2N-iFGFR1 (iFGFR1) or C2N-iFGFR2 (iFGFR2) cells were lysed in Laemmli buffer for whole cell lysates and immunoblotted using activation-specific phospho-Erk, total Erk, iFGFR, and α -tubulin antibodies. *D*, quantitation, by densitometry, of phospho-Erk protein levels as a percentage of α -tubulin levels. Fold increases of iFGFR1 over iFGFR2 are shown in parentheses. *E*, C2N, C2N-iFGFR1, or C2N-iFGFR2 cells were serum starved for 48 h, treated with serum or media control, and immunoblotted using β -actin or activation-specific phospho-Erk antibodies.

control M-F_v-2-E) in the tumorigenic and metastatic CaP line TRAMP-C2N to create C2N-iFGFR1, C2N-iFGFR2, and C2N-C and in the nontumorigenic line TRAMP-C1A to make C1A-iFGFR1 and C1A-C. Derived from the TRAMP model, TRAMP-C2N and TRAMP-C1A are subclones of TRAMP-C2 and TRAMP-C1 cell lines that have been hypothesized to reflect different stages of tumor progression (15, 23). Clones with comparable expression levels of iFGFR1 and iFGFR2 as determined by immunoblotting were chosen for all experiments.

Initially, to determine whether differences in autophosphorylation between C2N-iFGFR1 and C2N-iFGFR2 could explain the disparate effects of distinct FGFRs seen in previous studies (5, 6), we examined AP20187-induced tyrosine phosphorylation of iFGFRs (Fig. 1*B*). No phosphorylation over background was observed for either iFGFR1 or iFGFR2 after addition of serum, confirming their insulation from activation by serum FGFs or endogenous serum-activated receptors (Fig. 1*B*). Furthermore, 5 min after drug addition, we observed an equivalent increase in phosphorylation of both iFGFR1 and iFGFR2, suggesting that the opposing effects of each receptor on prostate tumors was likely mediated by downstream signaling pathways.

Based on a previous observation in PC12 cells between FGFR1 and FGFR3, in which FGFR1 signaling led to greater Erk activation (24), and the established importance of Erk in growth factor-induced proliferation, we reasoned that FGFR1 and FGFR2 may also differ with regard to Erk phosphorylation (Fig. 1*C*). Whereas both iFGFRs receptors were able to phosphorylate Erk within 5–15 min of CID administration, iFGFR1 signaling consistently led to an approximately 3-fold higher phosphorylation of Erk than iFGFR2 (Fig. 1*D*).

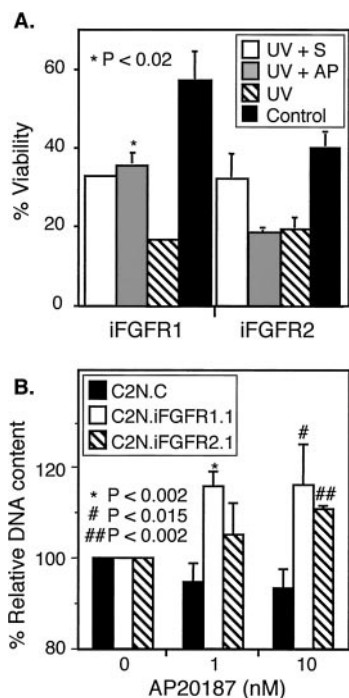


Fig. 2. *In vitro* activation of iFGFR1, but not iFGFR2, protects C2N cells from UV-induced cell death, whereas both iFGFRs can modestly induce proliferation. *A*, C2N.iFGFR1 and C2N.iFGFR2 cells were exposed to either 3 J or no UV (control) after 24 h in full media (S) or DMEM \pm 100 nM AP20187 (AP). Thereafter, cells were analyzed by trypan blue exclusion, and the proportion of cells excluding trypan blue was averaged from triplicate wells and plotted as a measure of cell survival. Probability was calculated by Student's *t* test between UV-treated C2N.iFGFR1 \pm 100 nM AP20187 (*, $P < 0.02$). This experiment is representative of three separate experiments. *B*, in a 96-well plate, duplicate wells of 5000 C2N.C, C2N.iFGFR1, or C2N.iFGFR2 cells were plated in DMEM with 0, 1, or 10 nM AP20187. Twenty-four h later, cultures were incubated with CyQUANT DNA dye, reflecting quantitative differences in DNA content and cell numbers. Probabilities were calculated by *t* test between values for C2N.iFGFR cell lines and C2N.C at the same AP20187 concentration (*, $P < 0.002$; #, $P < 0.015$; ##, $P < 0.002$). The average of three independent experiments is shown.

Additionally, Erk phosphorylation after treatment with serum for 15 min was 2.5-fold higher in C2N-iFGFR1 cells than in C2N-iFGFR2 cells. When compared with parental C2N cells, iFGFR1 and iFGFR2 showed no increase in background Erk phosphorylation (Fig. 1E). Thus, differential signaling to Erk by iFGFR1 and iFGFR2 may mirror the opposing effects attributed to these receptors in CaP.

Effects of iFGFR1 and iFGFR2 on Cell Death and Proliferation *in Vitro*. Numerous cellular effects have been attributed to the activation of FGFRs, including proliferation and survival. To determine the effects of iFGFR1 and iFGFR2 signaling on preventing cell death *in vitro*, we examined the ability of either iFGFR1 or iFGFR2 to protect cells from UV irradiation after serum starvation. The addition of either serum or 100 nM AP20187 led to a 2-fold increase in viable C2N-iFGFR1 cells after UV irradiation over untreated cells (Fig. 2A). In contrast, only serum could provide protection from UV for C2N-iFGFR2 cells. Thus, observed differences between iFGFR1 and iFGFR2 in their ability to protect cells from death after UV irradiation may underlie differences in tumor growth rates seen *in vivo*.

To complement these survival studies, we investigated changes in proliferation rates for C2N-iFGFR1, C2N-iFGFR2, and C2N-C cells. Cells were serum starved for 48 h in the presence or absence of 100 nM CID, and cell number was determined by multiple, independent approaches. In serum-free conditions, both iFGFRs could trigger a modest (12% increase) but reproducible proliferation, although no significant difference was seen between the two receptors (Fig. 2B). Thus, no significant difference between iFGFR1 and iFGFR2 signal-

ing on proliferation could be detected under *in vitro* growth conditions.

Influence of iFGFR1 on Tumor Initiation and Maintenance.

Due to the consistently observed ectopic expression of FGFR1 in human CaP and rodent CaP models, it was surprising that no major effects of FGFR1 signaling on proliferation and survival were observed *in vitro*. However, these *in vitro* studies may not adequately explore the contributions of the FGFR axis to CaP progression *in vivo*. To address this, we injected 2×10^6 C2N-iFGFR1.1 cells s.c. into the backs of syngeneic C57BL/6 mice. Two days later, we commenced biweekly i.p. injections of 50 μ g of AP20187, unless otherwise stated. Tumor volumes were estimated regularly with Vernier calipers. To distinguish between signaling leading to tumor establishment (or "take") versus tumor maintenance, we used three distinct drug regimens. In the first treatment group, AP20187 was administered continuously throughout the experiment to show the cumulative effects of iFGFR1 on tumor take and progression. In the second group, AP20187 was administered for the first 24 days. In the third group, AP20187 treatment was initiated 17 days after cell injections, and when well-established tumors (~ 200 mm³ at 42 days) appeared, CID administration was stopped. Also, to assess the normal baseline growth characteristics of clonal line C2N.iFGFR1.1 in mice, a fourth CID-free control growth curve was established.

In three independent experiments, differences in tumor growth were consistently observed between the control group and those mice that received continuous AP20187 (Fig. 3A). After 50 days of continuous CID treatment, tumors reached an average size of ~ 1600 mm³, whereas untreated tumors were ~ 90 mm³ at the same time point. Moreover, early and continuous CID treatment always (31 of 31 mice) led to tumor establishment compared with only $\sim 60\%$ (14 of 24 mice) in nontreated controls and 50% (5 of 10 mice) for parental C2N cells (Table 1; data not shown), demonstrating that FGFR1 signaling not only promoted growth but also contributed to tumor establishment or the ability of the cells to progress to a palpable size. Delaying drug

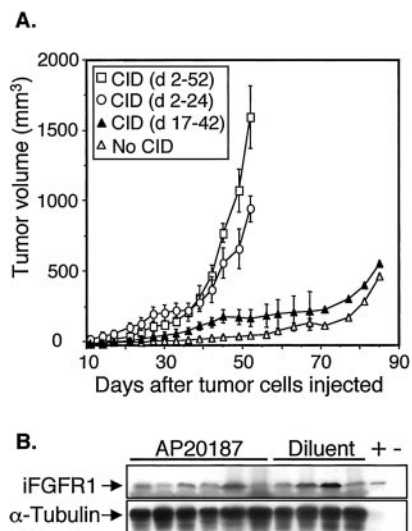


Fig. 3. Activation of iFGFR1 *in vivo* leads to increased tumor growth rates and iFGFR1/CID dependency for some tumors. *A*, 8–12-week-old C57BL/6 mice ($n = 5$) received s.c. injection with 2×10^6 C2N.iFGFR1.1 cells and were treated i.p. with different schedules (indicated by key, *d* = days) of biweekly AP20187 injection. Tumors were measured biweekly with Vernier calipers to estimate tumor volume using the formula $L \times W^2 \times 0.5236$ (where *L* is tumor length, and *W* is width). Graphs represent the mean volume \pm SD of five mice from each AP20187 regimen. The experiment is representative of three independent experiments. *B*, whole cell lysates of C2N-iFGFR1 tumors harvested from mice treated with continuous CID or mock treated were immunoblotted for the HA epitope tag of iFGFR1 (top panel) or α -tubulin (bottom panel). Control extracts are included from cells transiently transfected with iFGFR1 expression vector (+) or control vector (-).

Table 1 *Effects of iFGFRs on tumor initiation and progression*

Cell lines are indicated by type (TRAMP.C2N or C1A), the iFGFR expressed (iFGFR1 or iFGFR2), and as clone number (1 or 2) or noncloned "pooled" (P) stables. The indicated number of cells was injected from different cell lines into the backs of syngeneic C57BL/6 mice, and mice were treated biweekly with i.p. injections of AP20187 for the time courses indicated. Tumor volume was determined from Vernier caliper measurement, with the number of mice developing tumors above the minimum measurable size of 20 mm³ being listed.

Cell line	No. of cells injected	CID treatment ^a	Tumors (≥20 mm ³)
TRAMP.C2N	2 × 10 ⁶		5/10
TRAMP.C1A	2 × 10 ⁶		0/10
C2N.iFGFR1.1	2 × 10 ⁶	2–52	5/5
		2–24	5/5
		17–42	5/5
			3/5
C1A.iFGFR1.1	2 × 10 ⁶	4–52	0/5
		17–52	0/5
			0/5
C2N.iFGFR2.1	2 × 10 ⁶	2–52	0/5
		17–52	0/5
			0/5
C2N.iFGFR2.2	4 × 10 ⁶	2–56	0/10
		9–56	0/5
			0/10
C2N.iFGFR2.P	2 × 10 ⁶	2–45	0/6
			0/6

^a Days after injecting cells.

administration by 17 days did not alter the ultimate proportion of animals with tumors (100%), implying that the increased number of tumors observed after CID treatment was not due to greater early tumor survival but rather that some tumors required removal of a barrier to growth, possibly neoangiogenesis. Furthermore, when drug administration was delayed, growth was also consistently delayed in comparison with tumors continuously stimulated with AP20187.

Although CID treatment contributed to tumor growth and take, in most cases, tumors ultimately became CID independent. In both groups experiencing timed drug removal (*i.e.*, CID treatment on days 2–24 or 17–42), tumor growth temporarily stopped and even regressed in some animals (data not shown), revealing a role for iFGFR1 signaling in tumor maintenance. Nevertheless, most tumors (80%) were able to overcome iFGFR1 dependence and reestablished vigorous growth after an approximate 2-week delay (Fig. 3A). After this short latency period, the inability to resume rapid growth occurred only in the smallest tumors (data not shown), demonstrating that exogenous iFGFR1 signaling was not necessary for most TRAMP.C2N-derived tumors to grow.

Various explanations could account for escape from CID-dependent growth. Besides becoming completely independent of iFGFR1 signaling, tumors could theoretically escape AP20187 dependence by transgene amplification, leading to CID-independent iFGFR1 signaling. However, transgene immunoblotting revealed no consistent differences in average transgene expression between CID-treated and mock-treated tumors (Fig. 3B). Furthermore, when comparing mice that received drug continuously after tumor challenge with mice that received drug only at early time points, we observed only a slight delay in growth rates, reaching 1000 mm³ by days 48 and 50, respectively (Fig. 3A). This implies that iFGFR1 signaling is most critical for tumor take and early outgrowth but has diminished, if any, contribution to growth as tumors become relatively large and established.

To ascertain whether iFGFR1 signaling would be sufficient to drive tumor initiation and growth in nontumorigenic C1A cells, we injected C1A-iFGFR1.1 cells into the backs of mice and administered AP20187 starting 4 or 17 days later. In both CID-treated and untreated C1A-iFGFR1.1-injected mice, no tumors were detected up to 2 months after injection (Table 1). Thus, in the nontumorigenic

TRAMP.C1A line, iFGFR1 signaling was not sufficient for tumorigenesis or tumor take, demonstrating that iFGFR1 signaling is not sufficient to establish tumor growth in otherwise nontumorigenic cells. However, iFGFR1 can greatly augment tumor growth in already tumorigenic cell lines.

Influence of iFGFR2 on Tumor Initiation. In normal prostate epithelium, the FGFR2IIIb isoform of FGFR2 is widely expressed and responds to stromal-derived FGF-7 and FGF-10, leading to survival and differentiation of prostate epithelial cells. In previous studies, overexpression of FGFR2 kinase in Dunning rat-derived cell lines inhibited prostate tumor growth; however, these experiments could not rule out whether heterodimerization with endogenous FGFR1 (or other FGFRs) had occurred (5, 6). Additionally, in the Dunning model, prostate adenocarcinoma cells are mixed with stromal cells that likely provide additional factors that contribute to differentiation or inhibit proliferation of the epithelial cells. Although C2N cells are tumorigenic, injection of 2 × 10⁶ C2N-iFGFR2 cells did not lead to tumor growth under any drug treatment regimen (Table 1). Even when 4 × 10⁶ cells were injected, no drug-dependent (or independent) growth occurred.

To rule out the formal possibility that a clone-specific loss of tumorigenicity was responsible for these observations, we repeated the C2N.iFGFR2 experiment with both a second clone and also a "pooled" heterogeneous line of C2N-iFGFR2 cells. Again, consistent with previous reports, in all three experiments, no measurable iFGFR2-expressing C2N tumors developed (Table 1). It is clear that low-level basal signaling due to iFGFR2 expression is sufficient to inhibit tumor establishment; however, due to the absence of tumor growth, this model system cannot be used to ascertain whether FGFR2 signaling can inhibit or reverse the growth of established tumors.

FGFR1 Signaling *In Vivo* Augments Proliferation. Finally, we wanted to determine the underlying mechanism for the differential growth rates of iFGFR1-stimulated tumors. In the above-mentioned *in vivo* studies, we observed that once tumors achieved a certain size (~500 mm³; Fig. 3A), growth rates were indistinguishable regardless of iFGFR1 signaling. This was consistent with our immunohistochemistry of large (>1000 mm³) tumors excised at euthanasia, in which we saw no significant differences in proliferation (by Ki-67 staining), apoptosis (by terminal deoxynucleotidyltransferase-mediated nick end labeling assay), or vascularity (by CD31 signaling; data not shown). This contrasts with the result when CID-dependent iFGFR1 stimulation was terminated in relatively small (~200 mm³) tumors (Fig. 3A), in which growth rates declined with AP20187 withdrawal. Therefore, to attribute these growth rate differences to differential proliferation or apoptosis rates, we repeated a simplified version of the above C2N-iFGFR1 tumor experiment. After injecting 2 × 10⁶ C2N-iFGFR1.1 cells into 14 mice, we injected all mice with CID until tumors reached approximately 200 mm³ in size. Thereafter, half of the tumors were harvested. For the remaining animals, administration of AP20187 was terminated, and 6 days later, the remaining tumors were harvested. Unlike our results based on large, primarily CID-independent, tumors, loss of iFGFR1 signaling in small tumors led to a 2-fold reduction in proliferation rates based on Ki-67 staining (Fig. 4), but no changes in apoptosis (by terminal deoxynucleotidyltransferase-mediated nick end labeling assay) or vascularization (by CD31 staining) were detected (data not shown). Thus, whereas iFGFR signaling drives proliferation of moderately sized tumors (~200 mm³), it does not appear to influence apoptosis and angiogenesis in those tumors.

OPN Is Up-Regulated by iFGFR1 Signaling. After establishing that CID activation of iFGFR1 leads to increased tumor growth, we wanted to identify possible factors involved in the tumor-promoting effects of FGFR1. Therefore, we probed DNA microarray slides containing 6000 cDNAs to compare mRNA expression from 6-h

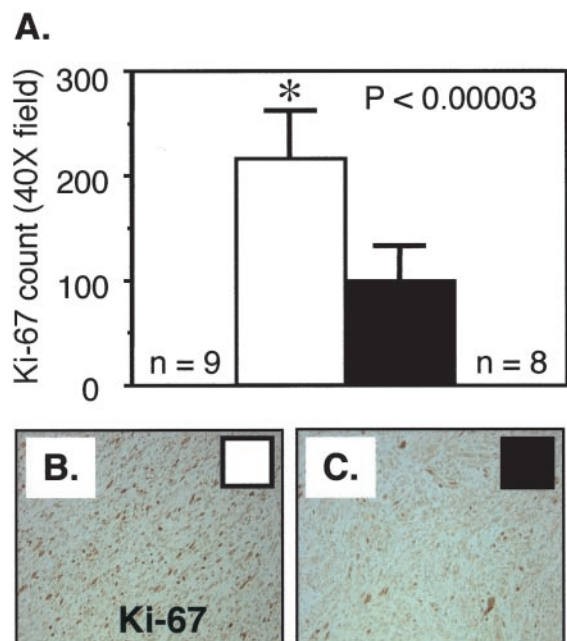


Fig. 4. Elimination of ectopic iFGFR1 signaling *in vivo* leads to a decrease in proliferation. C57BL/6 mice received injection with 2×10^6 C2N-iFGFR1.1 cells and were continuously treated with biweekly i.p. injections of AP20187 until tumors reached 200 mm³. Tumors were then harvested from nine mice, and CID was discontinued for the remaining animals, in which tumors were harvested 6 days later. Slides from paraffin-fixed tumors were analyzed by immunoperoxidase staining with antibodies to Ki-67. A, the mean of three random $\times 40$ fields of Ki-67-positive cells was averaged for the mice from each group. Representative fields of Ki-67-stained (methyl green counterstain) slides from mice continuously treated with AP20187 (B) or from mice with AP20187 removal (C) are shown.

CID-treated C2N-iFGFR1 cells with nontreated C2N-iFGFR1 cells. We focused on *OPN* for further analysis because it showed the strongest induction of any gene on the array. Interestingly, expression of *OPN* is thought to promote metastasis, especially to the bone, and serum levels of *OPN* are elevated in men with CaP (25–27). The microarray results were further validated by RNase protection assay using a time course of CID addition, revealing approximately 3-fold increases in CID-dependent *OPN* RNA levels (Fig. 5A) when normalized to α -tubulin levels (Fig. 5B). We also measure *OPN* protein levels by immunoblotting secreted *OPN* (Fig. 5C). At the protein level, we observed (by densitometry) a 4-fold increase in secreted *OPN* after iFGFR1 activation, whereas, in contrast, C2N-iFGFR2 cells had both lower basal levels of *OPN*, similar to parental cell lines (data not shown), and only very slight induction of *OPN*. Lending support to this finding, in a recent study, drug inhibition of FGFR1 and the Erk pathway blocked *OPN* expression in smooth muscle cells (28). Thus, in addition to demonstrating a dramatic difference in the signaling potential of FGFR1 *versus* FGFR2 *in vivo* at the cellular level, the CID system led to the identification of the tumor-associated *OPN* gene as a likely candidate for FGFR1-induced genes that can promote tumor growth.

DISCUSSION

In this study, we have applied CID technology to address crucial questions about the differences between FGFR1 and FGFR2 signaling on the development of CaP. In particular, we have explored the temporal role of FGFR1 signaling in tumor development and whether the signaling differences between FGFR1 and FGFR2 are quantitative or qualitative. Additionally, we have examined how FGFR1 influences tumor growth and what factors might mediate the effects of FGFR1 on tumor progression.

Using CID technology, we elucidated a quantitative signaling difference between the two receptors. Although we observed comparable activation of iFGFR1 and iFGFR2 by autophosphorylation, activation of Erk was 3-fold higher by iFGFR1 when compared with iFGFR2. However, in comparison with C2N.iFGFR1 cells, we also observed 2-fold lower Erk phosphorylation in C2N.iFGFR2 cells after addition of serum, implying that ectopic expression of iFGFR2 impedes Erk signaling in C2N cells independently of CID. This may help explain the loss of tumorigenicity of multiple clones of C2N.iFGFR2 cells we observed in our studies. In independent studies of human salivary adenocarcinoma-derived cells, expression of full-length FGFR2 blocked tumor growth and basally inhibited endogenous FGFR phosphorylation of FRS2, the major upstream substrate for FGFR activation of the Erk cascade (29). Although no mechanism was provided, an active suppression of FRS2 signaling due to FGFR2 expression is implied. Because FRS2 associates with FGFRs independently of receptor phosphorylation, overexpression of iFGFR2 may sequester FRS2 from endogenous FGFR1, thereby preventing Erk signaling.

The enhanced proliferation after iFGFR1 signaling in C2N.iFGFR1 cells *in vivo versus in vitro* suggests that FGFR1-induced genes may support mechanisms that can overcome barriers to tumor growth *in vivo*, such as neoangiogenesis, stromal independence, and anchorage independence. *OPN*, which we have shown to be differentially up-regulated by iFGFR1, has previously been shown to enhance anchorage independence (30) and facilitate tumor growth through increased proliferation (31), whereas *OPN*-specific antisense transcripts can retard tumor growth (32). Possibly *OPN* and/or other FGFR1-induced factors support the proliferation we observed *in vivo*.

Beyond ~ 0.5 mm in size, tumors become hypoxic without addi-

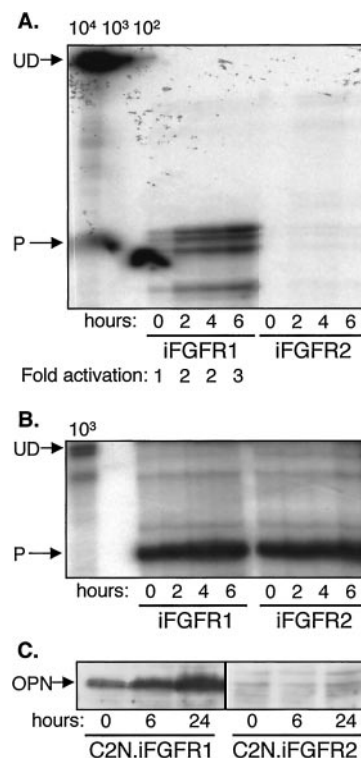


Fig. 5. Activation of iFGFR1, but not iFGFR2, leads to increased expression of *OPN* as well as secretion of *OPN* protein. A–C, C2N-iFGFR1 or C2N-iFGFR2 cells were serum starved and treated for the times indicated with 100 nM AP20187. A and B, total RNA was isolated from cells, and RNase protection was performed. Undigested (UD) probes and *OPN* (A) and β -actin (B) “protected” (P) RNA molecules were resolved on a denaturing polyacrylamide gel. C, media were collected and quantified by Bradford assay, and equal amounts of protein were separated by SDS-PAGE for immunoblotting with *OPN*-specific antibodies. Data are representative of at least three experiments.

tional vasculature (33). iFGFR1 signaling may help overcome this barrier to tumor establishment through proangiogenic signals, such as VEGF up-regulation or thrombospondin (TSP-1) inhibition (34), acting at a very early stage in tumor growth. This mechanism would not be expected to contribute to growth in culture where oxygen is abundant, consistent with our inability to observe changes in VEGF expression in C2N cells after iFGFR1 signaling *in vitro* (data not shown). Furthermore, this mechanism would be expected to be less important in already established well-vascularized tumors, consistent with our observations that iFGFR1 signaling leads to an increase in proliferation, but not to an increase in vasculature density in tumors 200 mm³ in size. Extrapolating from the effects of iFGFR1 signaling on tumors 200 mm³ in size and our additional observations based on transgenic mice expressing iFGFR1 in the prostatic epithelium, where vascularization occurs after a long period of hyperplasia,⁵ we conclude that neovascularization is secondary to proliferation in our model. A likely scenario is that iFGFR1 signaling stimulates proliferation, either via the Erk pathway or indirectly via OPN or other proteins, driving tumors growth beyond vascular capacity. This, in turn, would lead to hypoxia and the stabilization of hypoxia-inducible factor 1 α , a transcription factor that induces the expression of proangiogenic factors, such as VEGF. With sufficient paracrine signaling from hypoxic cells, rapidly dividing tumors would promote neoangiogenesis, allowing further growth (33). Although this would also occur within unmodified C2N-derived tumors, iFGFR1 signaling would augment this process, increasing both the rate of growth and the proportion of established tumors.

Although these experiments were conducted in the presence of endogenous FGFR1 signaling, additional ectopic iFGFR1 signaling also influenced tumor growth rates until the tumors were quite large (at least 200 mm³), vascularized, and well established. By blocking endogenous FGFR1 signals, an even greater role for FGFR1 signaling on tumor growth could be revealed. Additionally, the C2N cell line produces poorly differentiated tumors, with high genetic heterogeneity, potentially leading to more genetic resources for circumventing the loss of iFGFR1 signaling. Nevertheless, some tumors (20%) were still unable to overcome the loss of iFGFR1 signals, suggesting that therapies aimed at selectively blocking FGFR1 signaling might have dramatic consequences for a subset of prostate tumors.

As demonstrated here, CID technology can be a powerful tool in elucidating the roles of distinct signaling molecules in disease progression and for modeling CaP development. In a previous paper, we used iFGFR1 to create a mouse model with progressive transformation of the mammary gland (19). As a second step, creation of transgenic mice expressing inducible signaling molecules in the prostate epithelium and breeding these conditional models with established CaP models (*e.g.*, TRAMP) or to other cancer susceptibility models (*e.g.*, p53, Rb deficient) will allow for a more accurate determination of the temporal, additive, and synergistic roles of many signaling factors for tumor development, progression, and dissemination. This should permit the creation of "susceptibility maps," where tumor grade is correlated with susceptibility to loss of an inducible signaling pathway, thereby providing information into when therapeutics for that pathway would be most useful.

These studies show that FGFR signaling is important for the earliest stages of tumor establishment; however, FGFR1 involvement in other stages of cancer progression cannot be excluded. Additionally, FGFR1 promotes *in vivo* proliferation and transcriptionally up-regulates the metastasis-associated protein OPN. Also, using iFGFRs, we have shown that quantitative differences exist in signaling between

FGFR1 and FGFR2. We confirmed previous results by showing a positive contribution by FGFR1 signaling to prostate tumor growth and a negative effect by FGFR2 with the intracellular signaling domains of the receptors largely responsible for the opposing effects of FGFR1 and FGFR2 on tumor growth (5). Finally, we have used these CID-inducible receptors to better understand FGFR signaling in tumor establishment and maintenance, while illuminating the importance of FGFR1 signaling as an excellent target for CaP intervention and ectopic overexpression of FGFR2 as a potential gene therapy.

ACKNOWLEDGMENTS

We are grateful to Julie Zhao for technical assistance and members of the Spencer laboratory for helpful discussions.

REFERENCES

- Jemal, A., Murray, T., Samuels, A., Ghafoor, A., Ward, E., and Thun, M. J. Cancer statistics, 2003. *CA Cancer J. Clin.*, *53*: 5–26, 2003.
- Boilly, B., Vercoutter-Edouart, A. S., Hondermarck, H., Nurcombe, V., and Le Bourhis, X. FGF signals for cell proliferation and migration through different pathways. *Cytokine Growth Factor Rev.*, *11*: 295–302, 2000.
- Foster, B. A., Kaplan, P. J., and Greenberg, N. M. Peptide growth factors and prostate cancer: new models, new opportunities. *Cancer Metastasis Rev.*, *17*: 317–324, 1998.
- Naimi, B., Latil, A., Fournier, G., Mangin, P., Cussenot, O., and Berthon, P. Down-regulation of (IIb) and (IIIc) isoforms of fibroblast growth factor receptor 2 (FGFR2) is associated with malignant progression in human prostate. *Prostate*, *52*: 245–252, 2002.
- Feng, S., Wang, F., Matsubara, A., Kan, M., and McKeehan, W. L. Fibroblast growth factor receptor 2 limits and receptor 1 accelerates tumorigenicity of prostate epithelial cells. *Cancer Res.*, *57*: 5369–5378, 1997.
- Matsubara, A., Kan, M., Feng, S., and McKeehan, W. L. Inhibition of growth of malignant rat prostate tumor cells by restoration of fibroblast growth factor receptor 2. *Cancer Res.*, *58*: 1509–1514, 1998.
- Powers, C. J., McLeskey, S. W., and Wellstein, A. Fibroblast growth factors, their receptors and signaling. *Endocr. Relat. Cancer*, *7*: 165–197, 2000.
- Valve, E. M., Nevalainen, M. T., Nurmi, M. J., Laato, M. K., Martikainen, P. M., and Harkonen, P. L. Increased expression of FGF-8 isoforms and FGF receptors in human premalignant prostatic intraepithelial neoplasia lesions and prostate cancer. *Lab. Invest.*, *81*: 815–826, 2001.
- Kwabi-Addo, B., Ropiquet, F., Giri, D., and Ittmann, M. Alternative splicing of fibroblast growth factor receptors in human prostate cancer. *Prostate*, *46*: 163–172, 2001.
- Ozen, M., Giri, D., Ropiquet, F., Mansukhani, A., and Ittmann, M. Role of fibroblast growth factor receptor signaling in prostate cancer cell survival. *J. Natl. Cancer Inst.* (Bethesda), *93*: 1783–1790, 2001.
- Spencer, D. M., Wandless, T. J., Schreiber, S. L., and Crabtree, G. R. Controlling signal transduction with synthetic ligands. *Science (Wash. DC)*, *262*: 1019–1024, 1993.
- Spencer, D. M., Graef, I., Austin, D. J., Schreiber, S. L., and Crabtree, G. R. A general strategy for producing conditional alleles of Src-like tyrosine kinases. *Proc. Natl. Acad. Sci. USA*, *92*: 9805–9809, 1995.
- Blau, C. A., Peterson, K. R., Drachman, J. G., and Spencer, D. M. A proliferation switch for genetically modified cells. *Proc. Natl. Acad. Sci. USA*, *94*: 3076–3081, 1997.
- MacCorkle, R. A., Freeman, K. W., and Spencer, D. M. Synthetic activation of caspases: artificial death switches. *Proc. Natl. Acad. Sci. USA*, *95*: 3655–3660, 1998.
- Foster, B. A., Gingrich, J. R., Kwon, E. D., Madias, C., and Greenberg, N. M. Characterization of prostatic epithelial cell lines derived from transgenic adenocarcinoma of the mouse prostate (TRAMP) model. *Cancer Res.*, *57*: 3325–3330, 1997.
- Gingrich, J. R., and Greenberg, N. M. A transgenic mouse prostate cancer model. *Toxicol. Pathol.*, *24*: 502–504, 1996.
- Gingrich, J. R., Barrios, R. J., Morton, R. A., Boyce, B. F., DeMayo, F. J., Finegold, M. J., Angelopoulos, R., Rosen, J. M., and Greenberg, N. M. Metastatic prostate cancer in a transgenic mouse. *Cancer Res.*, *56*: 4096–4102, 1996.
- Huss, W. J., Hanrahan, C. F., Barrios, R. J., Simons, J. W., and Greenberg, N. M. Angiogenesis and prostate cancer: identification of a molecular progression switch. *Cancer Res.*, *61*: 2736–2743, 2001.
- Welm, B. E., Freeman, K. W., Chen, M., Contreras, A., Spencer, D. M., and Rosen, J. M. Inducible dimerization of FGFR1: development of a mouse model to analyze progressive transformation of the mammary gland. *J. Cell Biol.*, *157*: 703–714, 2002.
- Fan, L., Freeman, K. W., Khan, T., Pham, E., and Spencer, D. M. Improved artificial death switches based on caspases and FADD. *Hum. Gene Ther.*, *10*: 2273–2285, 1999.
- Greenberg, N. M., DeMayo, F., Finegold, M. J., Medina, D., Tilley, W. D., Aspinall, J. O., Cunha, G. R., Donjacour, A. A., Matusik, R. J., and Rosen, J. M. Prostate cancer in a transgenic mouse. *Proc. Natl. Acad. Sci. USA*, *92*: 3439–3443, 1995.
- Clackson, T., Yang, W., Rozamus, L. W., Hatada, M., Amara, J. F., Rollins, C. T., Stevenson, L. F., Magari, S. R., Wood, S. A., Courage, N. L., Lu, X., Cerasoli, F., Jr., Gilman, M., and Holt, D. A. Redesigning an FKBP-ligand interface to generate

⁵ Kevin W. Freeman and David M. Spencer, unpublished results.

- chemical dimerizers with novel specificity. *Proc. Natl. Acad. Sci. USA*, *95*: 10437–10442, 1998.
23. Han, G., Foster, B. A., Mistry, S., Buchanan, G., Harris, J. M., Tilley, W. D., and Greenberg, N. M. Hormone status selects for spontaneous somatic androgen receptor variants that demonstrate specific ligand and cofactor dependent activities in autochthonous prostate cancer. *J. Biol. Chem.*, *276*: 11204–11213, 2001.
 24. Raffioni, S., Thomas, D., Foehr, E. D., Thompson, L. M., and Bradshaw, R. A. Comparison of the intracellular signaling responses by three chimeric fibroblast growth factor receptors in PC12 cells. *Proc. Natl. Acad. Sci. USA*, *96*: 7178–7183, 1999.
 25. Fedarko, N. S., Jain, A., Karadag, A., Van Eman, M. R., and Fisher, L. W. Elevated serum bone sialoprotein and osteopontin in colon, breast, prostate, and lung cancer. *Clin. Cancer Res.*, *7*: 4060–4066, 2001.
 26. Angelucci, A., Festuccia, C., D'Andrea, G., Teti, A., and Bologna, M. Osteopontin modulates prostate carcinoma invasive capacity through RGD-dependent upregulation of plasminogen activators. *Biol. Chem.*, *383*: 229–234, 2002.
 27. Cooper, C. R., Chay, C. H., and Pienta, K. J. The role of $\alpha_v\beta_3$ in prostate cancer progression. *Neoplasia*, *4*: 191–194, 2002.
 28. Li, G., Oparil, S., Kelpke, S. S., Chen, Y. F., and Thompson, J. A. Fibroblast growth factor receptor-1 signaling induces osteopontin expression and vascular smooth muscle cell-dependent adventitial fibroblast migration *in vitro*. *Circulation*, *106*: 854–859, 2002.
 29. Zhang, Y., Wang, H., Toratani, S., Sato, J. D., Kan, M., McKeehan, W. L., and Okamoto, T. Growth inhibition by keratinocyte growth factor receptor of human salivary adenocarcinoma cells through induction of differentiation and apoptosis. *Proc. Natl. Acad. Sci. USA*, *98*: 11336–11340, 2001.
 30. Thalmann, G. N., Sikes, R. A., Devoll, R. E., Kiefer, J. A., Markwalder, R., Klima, I., Farach-Carson, C. M., Studer, U. E., and Chung, L. W. Osteopontin: possible role in prostate cancer progression. *Clin. Cancer Res.*, *5*: 2271–2277, 1999.
 31. Philip, S., Bulbule, A., and Kundu, G. C. Osteopontin stimulates tumor growth and activation of promatrix metalloproteinase-2 through nuclear factor- κ B-mediated induction of membrane type 1 matrix metalloproteinase in murine melanoma cells. *J. Biol. Chem.*, *276*: 44926–44935, 2001.
 32. Gardner, H. A., Berse, B., and Senger, D. R. Specific reduction in osteopontin synthesis by antisense RNA inhibits the tumorigenicity of transformed Rat1 fibroblasts. *Oncogene*, *9*: 2321–2326, 1994.
 33. Giatromanolaki, A., and Harris, A. L. Tumour hypoxia, hypoxia signaling pathways and hypoxia inducible factor expression in human cancer. *Anticancer Res.*, *21*: 4317–4324, 2001.
 34. Doll, J. A., Reiher, F. K., Crawford, S. E., Pins, M. R., Campbell, S. C., and Bouck, N. P. Thrombospondin-1, vascular endothelial growth factor and fibroblast growth factor-2 are key functional regulators of angiogenesis in the prostate. *Prostate*, *49*: 293–305, 2001.